Journal of Systems Engineering and Electronics
Vol. 33, No. 4, August 2022, pp.835 – 844

Navigation jamming signal recognition based on long short-term memory neural networks

FU Dong, LI Xiangjun, MOU Weihua*, MA Ming, and OU Gang

College of Electronic Science and Technology, National University of Defense Technology, Changsha 410005, China

Abstract: This paper introduces the time-frequency analyzed long short-term memory (TF-LSTM) neural network method for jamming signal recognition over the Global Navigation Satellite System (GNSS) receiver. The method introduces the long short-term memory (LSTM) neural network into the recognition algorithm and combines the time-frequency (TF) analysis for signal preprocessing. Five kinds of navigation jamming signals including white Gaussian noise (WGN), pulse jamming, sweep jamming, audio jamming, and spread spectrum jamming are used as input for training and recognition. Since the signal parameters and quantity are unknown in the actual scenario, this work builds a data set containing multiple kinds and parameters jamming to train the TF-LSTM. The performance of this method is evaluated by simulations and experiments. The method has higher recognition accuracy and better robustness than the existing methods, such as LSTM and the convolutional neural network (CNN).

Keywords: satellite navigation, jamming recognition, time-frequency (TF) analysis, long short-term memory (LSTM).

DOI: 10.23919/JSEE.2022.000083

1. Introduction

The global navigation satellite system (GNSS) is widely utilized in an abundance of applications. Critical infrastructures such as cellular towers, the power grid and even financial trading institutions can be disrupted if the GNSS receivers are jammed. Accurate recognition of navigation jamming signals is the premise of monitoring and suppression. However, jamming signal identification with high accuracy is not an easy task at present.

Traditional navigation jamming signal classifiers are designed based on the time, frequency or time-frequency (TF) domain features of the signal. The threshold determination and implementation of the algorithm are complex, and its performance in a low signal to noise ratio (SNR) is not satisfactory [1−3]. The shallow neural network is also used to recognize the jamming signal in recent years. Mosavi et al. [4] used multi-layer perceptron for narrowband jamming tracking and suppression, it cannot recognize other types of jamming signals. Wang et al. [5] classified jamming signals based on back propagation (BP) neural network, but the jamming existence factor, bandwidth, spectral kurtosis, and average spectral flatness coefficient are required.

Deep neural network (DNN) including convolutional neural network (CNN) and recurrent neural network (RNN) has been widely used in signal processing and recognition. A large number of studies show how to use CNN to classify jamming signals in communication systems [6−10], or to classify transient radio frequency interference [11]. In addition, CNN is also widely used in signal modulation recognition [12,13], time series classification [14], and image target classification [15]. The long short-term memory (LSTM) neural network is proposed to solve the problem of gradient disappearance and explosion in the training process of ordinary RNN [16]. It is better at learning the dependence between signal sequences than other RNN, such as solar radio spectrum, machine fault diagnosis [17], abnormal electrocardiogram signals [18,19]. Moreover, LSTM is also used for signal modulation identification [9,20]. In terms of jamming recognition, LSTM is used for radar emitter [21] and wireless interference signal recognition [8,22], radio frequency signal classification [23].

The recent success of DNN in jamming classification in other fields suggests that the recognition of navigation jamming can benefit from it. Thus, researchers start using CNN in the navigation, but the case of using LSTM has not been found. Wu. et al [24] used one-dimensional CNN to extract jamming signal features for classification. However, retraining CNN under different parameter conditions seriously limits the practicability of the method. The adaptability of CNN to the variation of jamming signal parameters such as the period of pulse jamming, the

Manuscript received March 05, 2021.
*Corresponding author.
This work was supported by the National Natural Science Foundation of China (62003354).

frequency sweep rate of sweep jamming, etc., has not been discussed. Li et al. [25] used the smooth pseudo Wigner-Ville distribution to convert jamming signals into images, then extracted image features for recognition with CNN. Although the method can classify signals in a certain range of parameters, it takes a lot of memory and signal processing resources.

This paper proposes a method named TF-LSTM to recognize navigation jamming signals with high accuracy in real scenarios. This idea is based on two facts:

(i) The jamming signal varies continuously and dependently over time, and provides an opportunity for the application of LSTM.

(ii) TF can extract signal parameters for jamming suppression and enhance signal features [2,3].

Our contributions include the following:

(i) The LSTM is introduced into the navigation jamming recognition and the TF is used for signal preprocessing.

(ii) For the first time, the adaptability of the recognition method to the range of navigation jamming signal parameters is researched.

(iii) Several groups of comparative studies prove the advantages of the new method in recognizing single and multiple jamming signals over a wide range of parameter variations in actual scenarios.

The model of the jamming signal recognition system is introduced in Section 2, as well as the mathematical model of the navigation jamming signal. This work explains the principles of TF analysis, LSTM and signal feature extraction in Section 3. The performance of different methods is discussed by simulations and experiments in Section 4.

2. System description

2.1 System model

The GNSS user receives a radio frequency (RF) signal within a certain bandwidth, obtains an intermediate frequency signal through down-conversion and filtering, then performs acquisition and tracking. The jamming still exists in the intermediate frequency (IF) signal after down-conversion if there are jamming signals in the received bandwidth, so the recognition of the navigation jamming signals can be completed within the IF bandwidth. The principle of the navigation jamming signal recognition system designed in this paper is shown in Fig. 1, which consists of a signal collection module and a signal analysis module. The collection module receives the signal through the antenna, converts the RF signal by down-conversion, sampling and quantization into a digital IF signal stream, then sends it to the analysis module through the network protocol. After pre-processing the signal by TF analysis, the signal analysis module runs the recognition algorithm by using the trained neural network parameters, and performs operations including recording and early warning according to the classification results to provide reference for the subsequent jamming mitigation module. The functions in the blue dashed box are implemented by LSTM neural network.

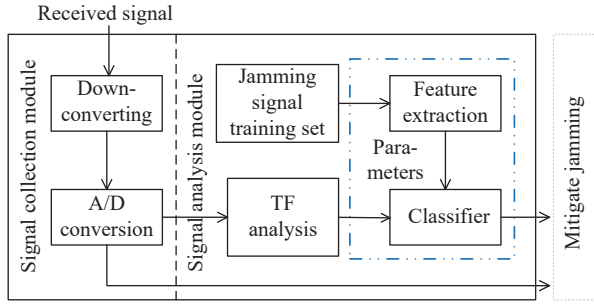

Fig. 1 Navigation jamming signal recognition system

2.2 Jamming signal model

The RF signal received by the antenna is expressed as

$$R(t) = S(t) + J(t) + n(t) \tag{1}$$

where $S(t)$ is the navigation signal in the frequency band, $J(t)$ is the jamming signal, and $n(t)$ is the noise in the environment. Since the navigation signal power is much lower than the noise and the jamming signal, this work focuses on the power relationship between the jamming signal and the noise, which is measured by the jamming to noise ratio (JNR).

The navigation jamming signals researched in this work include pulse jamming, sweep jamming, audio jamming, and spread spectrum jamming.

Pulse jamming is a kind of jamming obtained by modulating a pulse signal to a single frequency carrier, the pulse signal is in the form of a square wave, its time-domain signal expression is

$$J_p(t) = \sum_{n=-\infty}^{+\infty} p_\tau(t - nT) A_p \exp(\mathrm{j}2\pi f_p t + \varphi_p) \tag{2}$$

where τ and T are the pulse width and repetition period; A_p,f_p, and $\varphi_p$are the amplitude, frequency, and initial phase of the carrier respectively.

Sweep jamming in this paper changes the centre frequency linearly with time. In addition, its amplitude may also change with time in some cases, and it can cover a larger bandwidth in the frequency domain within a period of time. The time domain signal expression is

$$J_s(t) = A_s \mathrm{rect}\left(\frac{1}{T}\right)\exp[\mathrm{j}2\pi\ (f_0 + Kt)t] \tag{3}$$

where A_s is the signal amplitude, T is the dwell time of a certain frequency point, f_0 is the initial frequency, and K is the constant coefficient of frequency change with time.

Audio jamming refers to a cosine signal with a single frequency that can interfere with a certain frequency point. It is the basic form of multi-tone jamming. The time domain expression is

$$J_a = A_a \exp(\mathrm{j}2\pi f_a t + \varphi_a) \tag{4}$$

where A_a, f_a, and φ_a are the jamming signal amplitude, frequency, and initial phase respectively. The difference in the initial phase generally does not cause the jamming effect to change.

Spread spectrum jamming usually refers to direct sequence spread spectrum (DSSS) signals. Depending on the spreading code rate, the navigation signal at the target frequency point will cause narrowband or wideband jamming. The time domain signal expression is

$$J_D = A_D C(t)\exp(\mathrm{j}2\pi f_D t + \varphi_D) \tag{5}$$

where $C(t)$ is the spreading code of carrier modulation. A_D, f_D, and φ_D are the amplitude, frequency, and phase of the carrier respectively.

3. Recognition algorithm

Inspired by mechanical fault diagnosis methods [26], this work uses TF analysis to strengthen signal features, then LSTM is used to extract them.

3.1 TF analysis

TF analysis transforms the signal from the time domain to the TF domain. Signal features are similar in the time or frequency domain, which sometimes can be easily distinguished in the TF domain. The TF analysis methods used in this paper include the instantaneous frequency and the spectral entropy.

The instantaneous frequency of a non-stationary signal is a parameter that changes with time and is related to the average value of the frequencies present in the signal. When calculating the instantaneous frequency, using the short-time Fourier transform to calculate the TF power spectrum matrix $\boldsymbol{S}(t,f)$ of the input signal first, the number of rows is equal to the number of discrete Fourier transform (DFT) points, the number of columns $k = \lfloor (N_x - L)/(M - L) \rfloor$, N_x represents the length of the original signal, and $\lfloor x \rfloor$ represents rounding x down. Therefore, the $\boldsymbol{S}(t,f)$ matrix is expressed as

$$\boldsymbol{S}(t,f) = [X_1(f), X_2(f), \cdots, X_k(f)]. \tag{6}$$

The mth element in $\boldsymbol{S}(t,f)$ is

$$X_m(f) = \sum_{n=-\infty}^{\infty} x(n)\, g(n - mR)\, \mathrm{e}^{-\mathrm{j}2\pi n f} \tag{7}$$

where $x(n)$ is a discrete time domain signal, $g(n)$ is the window function of M point length, and $X_m(f)$ is the DFT of the data in the window centre on time mR. R is the number of data points skipped between two consecutive DFT. Its size is the difference between the window length M and the overlap length L. Then the instantaneous frequency is estimated [27,28] as

$$f_{\mathrm{inst}}(t) = \frac{\int_0^{\infty} f\boldsymbol{S}(t,f)\,\mathrm{d}f}{\int_0^{\infty} \boldsymbol{S}(t,f)\,\mathrm{d}f}. \tag{8}$$

The spectral entropy of a signal is a measure of its spectral power distribution. The spectral entropy regards the normalized power distribution of the signal in the frequency domain as a probability distribution and calculates its information entropy. The information entropy is the spectral entropy in this case [29,30]. For signal $x(n)$, if the TF power spectrum $\boldsymbol{S}(t,f)$ is known, the probability distribution $\boldsymbol{P}(m)$ is

$$\boldsymbol{P}(m) = \frac{\sum_t \boldsymbol{S}(t,m)}{\sum_f \sum_t \boldsymbol{S}(t,f)} \tag{9}$$

where $\boldsymbol{S}(t,m)$ is the TF power spectrum at a certain frequency m, then the spectral entropy is

$$H = -\sum_{m=1}^{N} \boldsymbol{P}(m)\log_2 \boldsymbol{P}(m). \tag{10}$$

The probability distribution of the given TF power spectrum $\boldsymbol{S}(t,f)$ at t is

$$\boldsymbol{P}(t,m) = \frac{\boldsymbol{S}(t,m)}{\sum_f \boldsymbol{S}(t,f)}. \tag{11}$$

Then the spectrum entropy at t is

$$H(t) = -\sum_{m=1}^{N} \boldsymbol{P}(t,m)\log_2 \boldsymbol{P}(t,m). \tag{12}$$

Calculate the instantaneous frequency and the spectral entropy of the non-jamming white Gaussian noise (WGN), pulse jamming, sweep jamming, audio jamming and spread spectrum jamming respectively in IF bandwidth. The TF analysis can be regarded as data pre-processing before LSTM training. As can be seen from Fig. 2, the pre-processing strengthens the features of the jamming signal. The jamming signal parameters are shown in Table 1. As shown in Fig. 2, the top of each panel is the original time-domain sequence, the middle

and the bottom of each panel are the instantaneous frequency and the spectral entropy sequences respectively. It can be seen that the feature between the time domain sequences of different signals is not obvious.

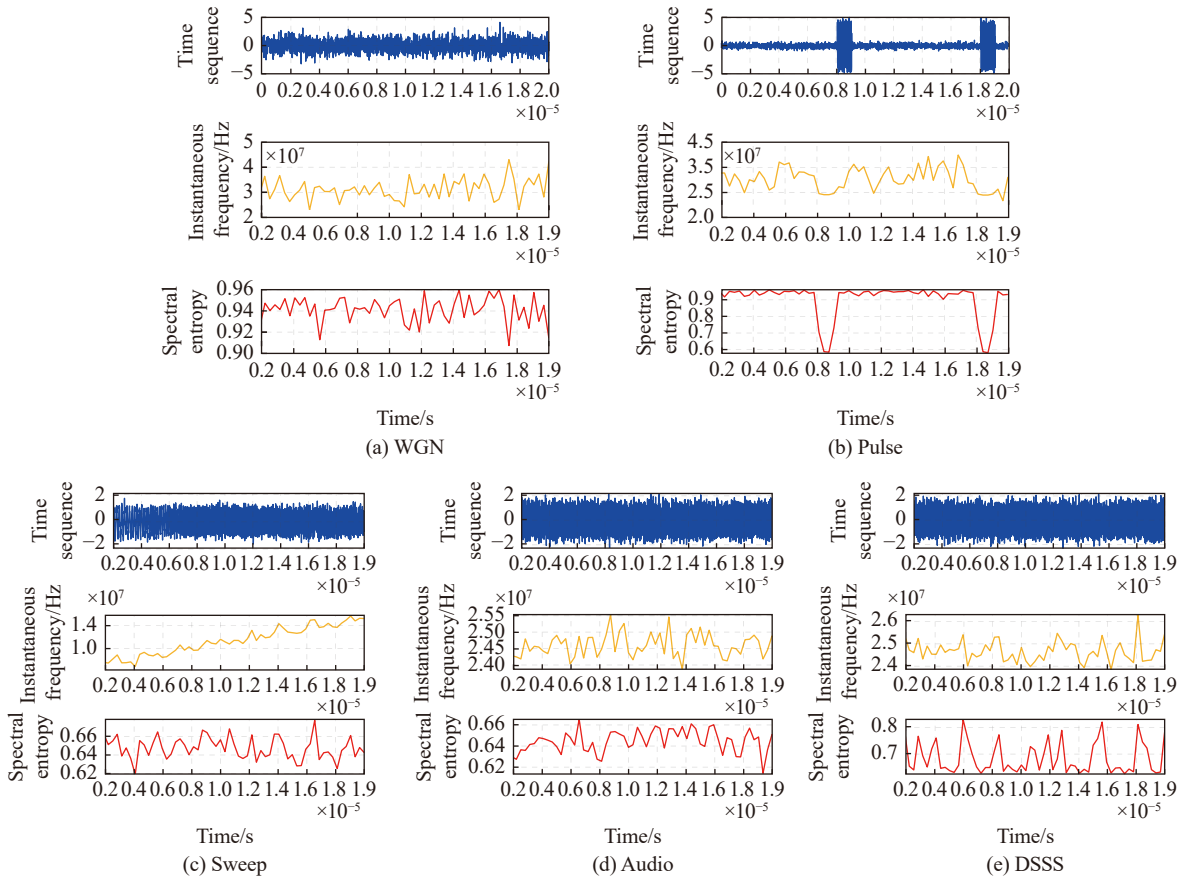

Fig. 2 TF analysis results of jamming signals

Table 1 Jamming signal parameters

Parameter	Value
JNR/dB	10
IF/MHz	24
Pulse jamming period/μs	10
Duty cycle/%	10
Sweep jamming bandwidth/MHz	40
Audio jamming frequency/MHz	1 575.42
Spread spectrum jamming carrier frequency/MHz	1 575.42
Code rate/Mcps	2.046

However, for the instantaneous frequency sequence, there are significant differences between jamming signals. WGN has a wider distribution in the frequency domain than other jamming signals, so the sequence fluctuates in a large range. In a pulse period of pulse jamming, the value of instantaneous frequency alternates between noise and carrier frequency. Sweep jamming linearly increases or decreases the instantaneous frequency with time. The frequency of audio jamming remains constant for a long time. The instantaneous frequency of spread spectrum jamming fluctuates around the carrier frequency, the higher code rate, and the larger range occupied for the sequence.

It is the same for the spectral entropy sequence. The sequence value of WGN is the largest. For pulse jamming, when there is a signal in the pulse period, the spectrum entropy mainly depends on the spectrum entropy of the carrier or it is similar to the spectrum entropy of noise. Change of frequency basically does not affect the power distribution for sweep jamming. For spread spectrum jamming, the value of the sequence between audio jamming and white noise is significantly different from other jamming signals.

Combining the two TF sequences will be benefit to distinguish the features of the jamming signal than the time domain sequences. The advantages of TF analysis is be shown in simulation and experiment.

3.2 LSTM neural networks

The standard RNN has a chain structure of repeating neural network modules, and there is only one nonlinear tanh function layer inside the repeating module, while the repeating module of LSTM has a more complex structure. The internal structure of each cell of the LSTM is shown in Fig. 3.

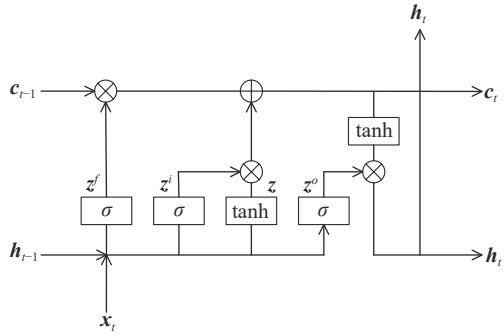

Fig. 3 LSTM cell structure

In Fig. 3, $\otimes$ is Hadamard multiplication, that is, the corresponding elements in the matrix are multiplied. $\oplus$ is matrix addition. The working principle of LSTM mainly has the following four parts:

(i) Decide to discard information. The first step in LSTM is to determine the information discarded from the cell state, which is determined by a forget gate gating signal:

$$\boldsymbol{z}^f = \sigma\left(\boldsymbol{W}^f \cdot [\boldsymbol{h}_{t-1}, \boldsymbol{x}_t]^{\mathrm{T}} + \boldsymbol{b}^f\right) \tag{13}$$

where $\boldsymbol{z}^f$ is the splicing vector multiplied by the weight matrix, and then converted to a number between 0 and 1 through a sigmoid activation function as the gated state of the forgotten gate. 1 means completely reserved, and 0 means completely discarded.

(ii) Confirm the update information. The next step is to determine the new information stored in the cell state. There are two parts. The first part is the input data, which creates an updated candidate value vector, and the second part is the calculation of the input gate, which determines whether the input data in the first part is updated:

$$\boldsymbol{z} = \tanh\left(\boldsymbol{W} \cdot [\boldsymbol{h}_{t-1}, \boldsymbol{x}_t]^{\mathrm{T}} + \boldsymbol{b}\right), \tag{14}$$

$$\boldsymbol{z}^i = \sigma\left(\boldsymbol{W}^i \cdot [\boldsymbol{h}_{t-1}, \boldsymbol{x}_t]^{\mathrm{T}} + \boldsymbol{b}^i\right), \tag{15}$$

where $\boldsymbol{z}^i$ is the state of the update gate, $\boldsymbol{z}$ is the value between −1 and 1 after the splicing vector is multiplied by the weight and converted into a value between −1 and 1 through the tanh activation function, which is used as the input data of the module, and the two together generate an update to the state.

(iii) Update the cell status. The first two steps have determined the upcoming operation, and this step is actually completed. Take the old state $\boldsymbol{c}_{t-1}$ Hadamard multiplicate $\boldsymbol{z}^f$, as discard the information determined to be discarded in (i), then add the updated information jointly determined by the two parts in (ii) to obtain the new state value $\boldsymbol{c}_t$ as

$$\boldsymbol{c}_t = \boldsymbol{c}_{t-1} \otimes \boldsymbol{z}^f + \boldsymbol{z} \otimes \boldsymbol{z}^i. \tag{16}$$

(iv) Confirm the output information. The output also includes two parts: one is based on the updated cell state to create the output candidate value vector, the other is to calculate the gated state of the output gate. The two parts jointly determineing the output information are

$$\boldsymbol{z}^o = \sigma\left(\boldsymbol{W}^o \cdot [\boldsymbol{h}_{t-1}, \boldsymbol{x}_t]^{\mathrm{T}} + \boldsymbol{b}^o\right), \tag{17}$$

$$\boldsymbol{h}_t = \boldsymbol{z}^o \otimes \tanh(\boldsymbol{c}_t), \tag{18}$$

where $\boldsymbol{z}^o$ is the state of the output gate; $\boldsymbol{h}_t$ is the final output data obtained by Hadamard multiplication of $\boldsymbol{z}^o$ and $\boldsymbol{c}_t$ through the tanh activation function.

The cell state is similar to a conveyor belt, with only a few linear interactions, so it is easy for the information to be transmitted on it to remain unchanged. LSTM removes or adds information to the cell state, useful features are remembered and useless features are forgotten. There are usually two chain structures of the LSTM neural network: one is the LSTM layer composed of ordinary unidirectional chains, and the other is the bidirectional LSTM (BiLSTM) layer combined of forward and backward chain. BiLSTM is more conducive to sequence features extraction [31].

The LSTM network contains five layers including a sequence input layer and a class output layer. The two input sequences are obtained by pre-processing the original jamming signal by the TF analysis in Subsection 3.1. The second layer is BiLSTM containing 200 cells (100 forward and 100 backward), the output of the BiLSTM layer goes through a fully connected layer. The fully connected layer connects each node output by the BiLSTM with each node of the softmax layer. After two layers' operation, jamming signal features are extracted from the input. Then the softmax layer is used which can achieve good classification. In softmax regression, the probability that we classify input x into category j is calculated by

$$p(y = j|x;\boldsymbol{\theta}) = \frac{\mathrm{e}^{\boldsymbol{\theta}_j^{\mathrm{T}} x}}{\sum_{l=1}^{k} \mathrm{e}^{\boldsymbol{\theta}_l^{\mathrm{T}} x}} \tag{19}$$

where $\boldsymbol{\theta}$ is the parameter of our model and k is the total class number. The softmax classifier calculates the exponent of each probability that the input belongs to each

category and normalizes all exponential probability. It is widely used for classification problems. The specific parameters of the network are shown in Table 2.

Table 2 LSTM neural network structure parameters

Layer	Type	Parameter
1	BiLSTM	200
2	Fully connected	5
3	Softmax	5

4. Simulation and experiment

The simulation and experiment use the same training and testing samples to compare the performance of CNN, LSTM, and TF-LSTM. The structure parameters of CNN refer to [24] and LSTM just has no time-frequency analysis part compared with TF-LSTM.

4.1 Simulation results and discussion

4.1.1 Neural network training

The jamming signal for neural network training is generated according to the signal model in Subsection 2.2. In addition, WGN is regarded as non-jamming to detect the existence of other jamming signals. The jamming signal parameters are as follows:

(i) Jamming types: WGN, pulse jamming, sweep jamming, audio jamming, and spread spectrum jamming.

(ii) JNR range: −5 dB to 15 dB.

(iii) Other parameters: the sample frequency is 125 MHz. The IF is 24 MHz. Pulse jamming: the pulse period T is between 1 μs and 1 ms, the duty cycle τ/T is 10%. Sweep jamming: the sweep frequency is between 1 555.42 MHz and 1 575.42 MHz, the sweep rate K is between 0.4 MHz/s and 400 MHz/s. Audio jamming: the carrier frequency f_a is randomly generated between 1 555.42 MHz and 1 575.42 MHz. Spread spectrum jamming: $C(t)$ is binary phase shift keying modulation, and the code rate is between 0.204 6 Mcps and 10.23 Mcps.

(iv) Signal samples: the sample length is 10 240 points. Each kind of the jamming signal has 1 000 training samples. There are a total of 5 × 1 000 = 5 000 training samples. Randomly select JNR and other parameters.

In order to test the recognition accuracy of different methods, this work uses the following test samples:

(i) The JNRs of the test sample are −5 dB, 0 dB, 5 dB, 10 dB, and 15 dB respectively. Other parameters are selected randomly and the range is the same as the training samples. There are a total of 5 × 5 × 1 000 = 25 000 samples.

(ii) The JNR of the test sample is randomly generated between −5 dB and 15 dB. Pulse jamming, sweep jamming, and spread spectrum jamming parameters are shown in Table 3. There are a total of 4 × 3 × 1 000 = 12 000 samples.

Table 3 Simulation jamming signal parameters

Jamming type	Parameter	Case 1	Case 2	Case 3	Case 4
Pulse	Period/μs	1	10	100	1 000
Sweep	Sweep rate/(MHz/s)	0.4	4	40	400
DSSS	Code rate/Mcps	0.204 6	1.023	2.046	10.23

(iii) The JNR and other parameters of the multiple jamming signals in each test sample are selected randomly as (i). There are a total of 5 × 1 000 = 5 000 samples.

The test samples (i) correspond to the problem of JNR variations in the actual scenario, the test samples (ii) correspond to the blind classification problem where the jamming signal parameters are unknown, and the test samples (iii) mean multiple jammings appear at the same time in the actual scenario.

4.1.2 Recognition accuracy

In order to research the adaptability of different methods to JNR. Test and draw the recognition accuracy of CNN, LSTM and TF-LSTM under different JNRs in Fig. 4.

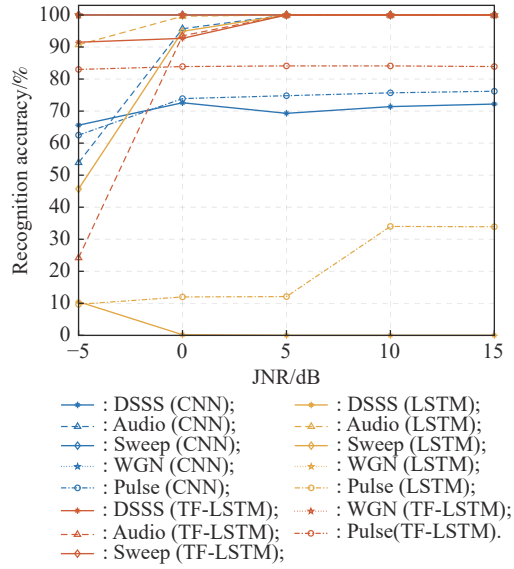

Fig. 4 JNR adaptability simulation recognition accuracy

It can be seen from Fig. 4 that with the increase of the jamming signal JNR, the recognition accuracy of the audio and pulse jamming increases. The recognition accuracy of spread spectrum jamming does not change significantly, and even with the increase of JNR, the accuracy decreases slightly. This is because CNN and LSTM extract noise as part of the DSSS feature during

training. The recognition accuracy of WGN and sweep is stable around 100%. It means that if there is jamming in the navigation frequency band, these methods can effectively detect it. Overall, the recognition accuracy of TF-LSTM for all jamming signals is higher than that of CNN and LSTM under different JNRs.

The adaptability of the different methods to jamming parameters is shown in Fig. 5. At the same time, we also test the recognition accuracy of the different methods in multiple jamming scenarios, the results can be seen in Fig. 6.

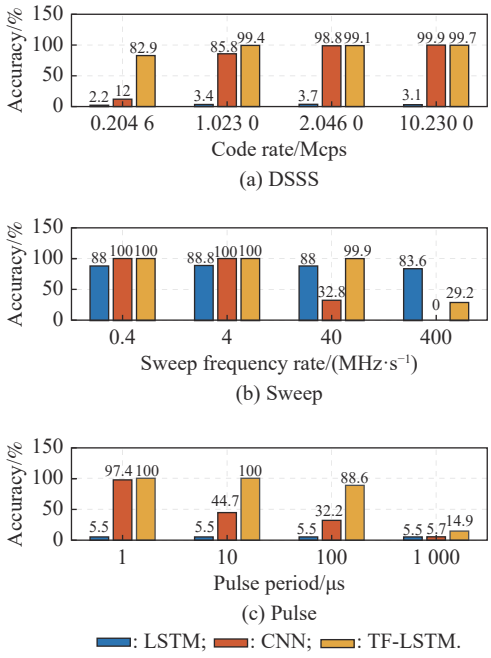

Fig. 5 Parameter adaptability simulation recognition accuracy

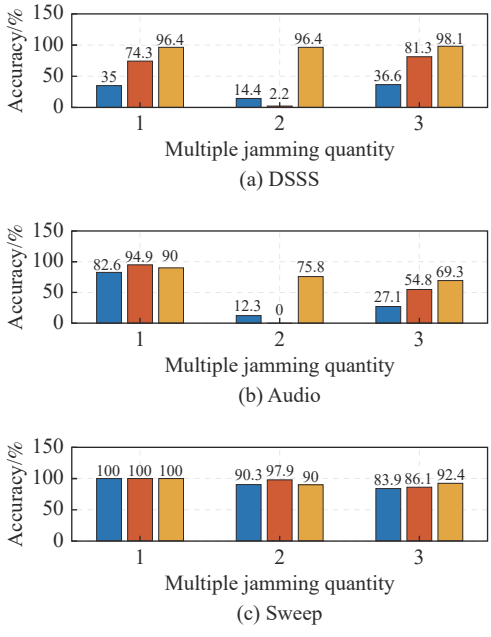

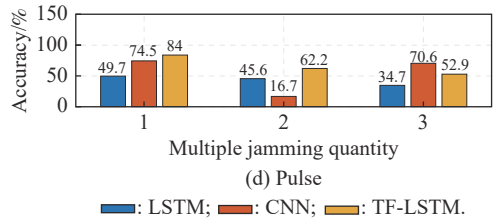

Fig. 6 Multiple jamming simulation recognition accuracy

Fig. 5 shows that there is a significant relationship between the recognition accuracy and the jamming parameters. The accuracy of pulse jamming is greatly reduced as the period reaches 1 ms for the three methods, because the sequence length corresponding to the excessive pulse period exceeds the feature extraction capability of CNN. Although the length of the sequence that LSTM can learn is limited, it still performs better than CNN. The sweep rate can be accurately identified in the order of 0.4 MHz/s—4 MHz/s for LSTM, but the sweep rate reaches 40 MHz/s or higher, its features are difficult to be extracted by CNN and TF-LSTM, especially CNN. When the code rate of spread spectrum jamming is lower than 1 Mcps, the recognition accuracy is significantly reduced for CNN. In addition, it is not possible to directly extract the sequence features for LSTM. Obviously, for the TF-LSTM, whether it is adaptable to JNR or other parameters, its performance is better than that of LSTM and CNN.

Fig. 6 illustrates that when multiple jammings appear at the same time, the recognition accuracy of CNN for each jamming signal changes dramatically, especially when two jammings appear, the LSTM also presents a similar result, while the recognition accuracy of TF-LSTM also decreases, but the decline is little, and the recognition accuracy is still the highest overall. It shows that the recognition accuracy of the three methods in the appearance of multiple jammings decreases to varying degrees, but the robustness and recognition accuracy of CNN and LSTM are not as good as TF-LSTM.

4.2 Experimental results and discussions

In this work, the experiment environment is placed in an open space. The platform of the jamming recognition research consists of receiving antennas, universal software radio peripheral (USRP) N300 and Laptop. The jamming signals are generated by a vector signal generator Agilent E4438C.

The jamming signal used for neural network training is collected by the instrument on the right in Fig. 7. The parameters of the jamming signal generated by Agilent E4438C are the same as those in the simulation part.

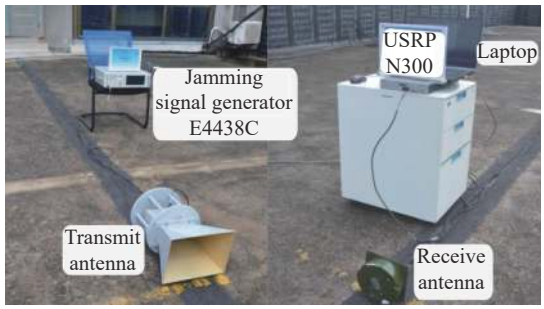

Fig. 7 Experiment scenario

4.2.1 Neural network training

In order to test the recognition accuracy of different methods, this work uses the following test samples:

(i) The JNRs of the test sample are −5 dB, 0 dB, 5 dB, 10 dB, and 15 dB respectively. Other parameters of jamming signals are randomly selected from Table 3, and there are a total of 5 × 5 × 1 000 = 25 000 samples.

(ii) The JNR of the test sample is randomly selected from −5 dB—15 dB. Pulse jamming, sweep jamming and spread spectrum jamming parameters are those in Table 3, and there are a total of 4 × 3 × 1 000 = 12 000 samples.

(iii) Limited by the experimental conditions, the JNR and other parameters of the two jamming signals in each test sample are traversed simultaneously from −5 dB to 15 dB and Table 3, respectively. There are a total of 5 × 1 000 = 5 000 samples.

4.2.2 Recognition accuracy

The recognition accuracy curve of the method under different JNRs is shown in Fig. 8. The recognition accuracy under different parameters is shown in Fig. 9. Meanwhile, Fig. 10 shows the multiple jamming recognition accuracy.

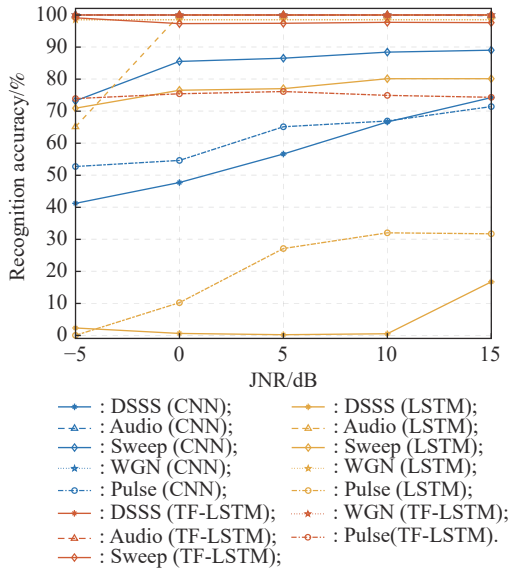

Fig. 8 JNR adaptability experimental recognition accuracy

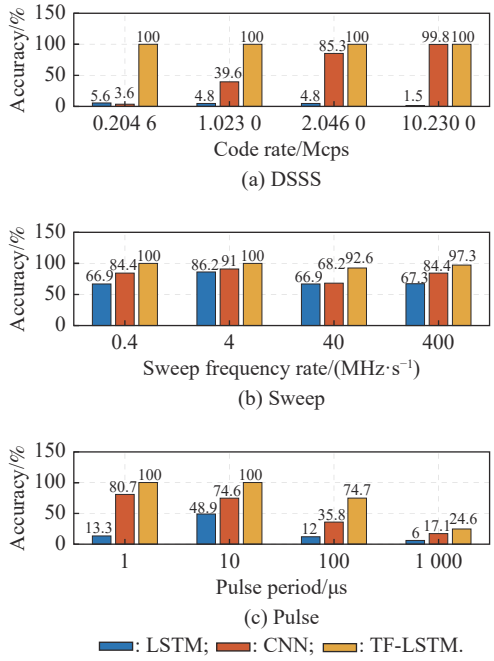

Fig. 9 Parameter adaptability experimental recognition accuracy

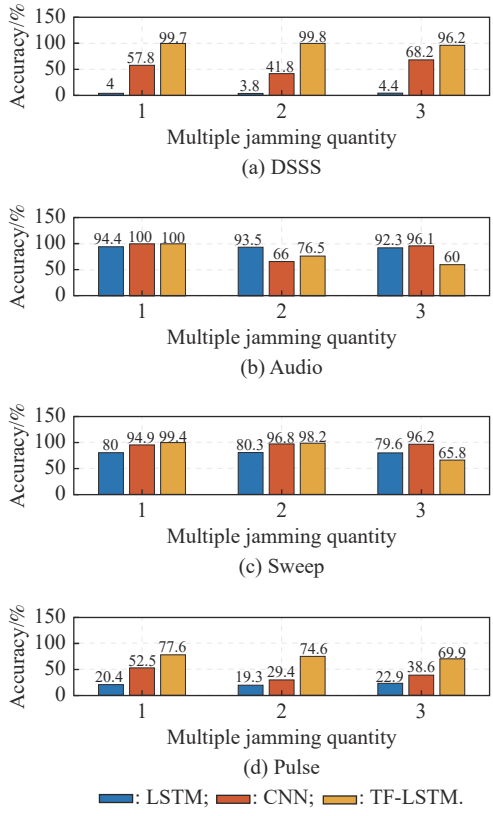

Fig. 10 Multiple jamming experimental recognition accuracy

It can be seen from Fig. 8 that with the increase of the jamming signal JNR, the recognition accuracy of most jamming signals is improved, and the recognition accuracy of WGN is still stable around 100%. In the experi-

mental scenario, the reflection of ground in the environment causes multipath signals and other effects, and the actual instrument is difficult to generate jamming signals consistent with the simulation, so the results of the experiment are slightly different from simulation. However, the recognition accuracy of TF-LSTM is still the highest.

The results in Fig. 9 also show that there is a significant relationship between the recognition accuracy and the jamming parameters. The accuracy of pulse and spread spectrum jamming is consistent with the simulation results. However, the recognition accuracy for the sweep jamming is different from the simulation, because when Agilent E4438C generates sweep signals, there is at least 1 ms dwell time at a certain frequency, which leads to the recognition accuracy of LSTM decreasing and CNN increasing under the same conditions. TF-LSTM is still robust to parameter variations in a wide range.

Fig. 10 illustrates that when multiple jammings appear, CNN and LSTM show certain similarity with the simulation results, but the recognition accuracy of audio jamming and sweep jamming is maintained high. The recognition accuracy of TF-LSTM decreases slowly with the increase of jamming quantity, but the accuracy and robustness of TF-LSTM in multiple jamming scenarios are still the best.

5. Conclusions

To solve the problem of navigation jamming signal recognition with unknown JNR and other parameters in actual scenarios, a method named TF-LSTM is proposed. The combination of TF and LSTM improves the recognition ability of the GNSS receiver, which will be beneficial to the jamming parameter estimation and mitigation in the future. Several groups of comparative experiments show that the recognition accuracy of TF-LSTM is higher than that of CNN and LSTM, and it is robust to jamming parameters variations in a wide range and multiple jammings.

References

[1] KANG C H, KIM S Y, PARK C G. A GNSS interference identification and tracking based on adaptive fading Kalman filter. Advanced Materials for Applied Science and Technology, 2014, 47(3): 3250–3255.

[2] AMIN M G, BORIO D, ZHANG Y D, et al. Time-frequency analysis for GNSSs: from interference mitigation to system monitoring. IEEE Signal Processing Magazine, 2017, 34(5): 85–95.

[3] WANG P, CETIN E, DEMPSTER A G, et al. GNSS interference detection using statistical analysis in the time-frequency domain. IEEE Trans. on Aerospace and Electronic Systems, 2017, 54(1): 416–428.

[4] MOSAVI M R, SHAFIEE, F. Narrowband interference suppression for GPS navigation using neural networks. GPS Solutions, 2016, 20(3): 341–351.

[5] WANG J X, CHANG Q, TIAN Y, et al. Research on GNSS interference signal detection method. Navigation Positioning and Timing, 2020, 7(4): 117–122.

[6] MAKARENKO A V. Deep learning algorithms for signal recognition in long perimeter monitoring distributed fiber optic sensors. Proc. of the 26th International Workshop on Machine Learning for Signal Processing, 2016. DOI: 10.1109/MLSP.2016.7738862.

[7] SCHMIDT M, BLOCK D, MEIER U. Wireless interference identification with convolutional neural networks. Proc. of the 15th International Conference on Industrial Informatics, 2017: 180–185.

[8] ZHANG X W, SEYFI T, JU S T, et al. Deep learning for interference identification: band, training SNR, and sample selection. Proc. of the 20th International Workshop on Signal Processing Advances in Wireless Communications, 2019. DOI: 101109/SPAWC.2019.8815481.

[9] ZHANG M, ZENG Y, HAN Z D, et al. Automatic modulation recognition using deep learning architectures. Proc. of the 19th International Workshop on Signal Processing Advances in Wireless Communications, 2018. DOI: 10.1109/SPAWC.2018.8446021.

[10] RIYAZ S, SANKHE K, IOANNIDIS S, et al. Deep learning convolutional neural networks for radio identification. IEEE Communications Magazine, 2018, 56(9): 146–152.

[11] CZECH D, MISHRA A, INGGS M. A CNN and LSTM-based approach to classifying transient radio frequency interference. Astronomy and Computing, 2018, 25: 52–57.

[12] YIN Z D, ZHANG R, WU Z L, et al. Co-channel multi-signal modulation classification based on convolution neural network. Proc. of the 89th Vehicular Technology Conference, 2019. DOI: 10.1109/VTCSpring.2019.8746292.

[13] YU J Y, ALHASSOUN M, BUEHRER R M. Interference classification using deep neural networks. Proc. of the IEEE 92nd Vehicular Technology Conference, 2020. DOI:10.1109/VTC2020-Fall49728.2020.9348658.

[14] ZHAO B D, LU H Z, CHEN S F, et al. Convolutional neural networks for time series classification. Journal of Systems Engineering and Electronics, 2017, 28(1): 162–169.

[15] LI B Q, HU X H. Effective distributed convolutional neural network architecture for remote sensing images target classification with a pre-training approach. Journal of Systems Engineering and Electronics, 2019, 30(2): 20–26.

[16] HOCHREITER S, SCHMIDHUBER J. Long short-term memory. Neural Computation, 1997, 9(8): 1735–1780.

[17] ZHAO R, YAN R Q, WANG J J, et al. Learning to monitor machine health with convolutional bi-directional LSTM networks. Sensors, 2017, 17(2): 273–290.

[18] YILDIRIM O. A novel wavelet sequences based on deep bi-directional LSTM network model for ECG signal classification. Computers in Biology and Medicine, 2018, 96: 189–202.

[19] KOSOWSKI G, RYMARCZYK T, WOJCIK D, et al. The use of time-frequency moments as inputs of LSTM network for ECG signal classification. Electronics, 2020, 9(9): 1452–1473.

[20] WEST N, O'SHEA T. Deep architectures for modulation recognition. Proc. of the International Symposium on Dynamic Spectrum Access Networks, 2017. DOI: 10.1109/DySPAN.2017.7920754.
[21] QIN Y, YANG J, ZHU M T, et al. Fast recognition of pull-off jamming using LSTM. Proc. of the IEEE International Conference on Signal, Information and Data Processing, 2019. DOI: 10.1109/ICSIDP47821.2019.9173490.
[22] MA J T, LIU H, PENG C, et al. Unauthorized broadcasting identification: a deep LSTM recurrent learning approach. IEEE Trans. on Instrumentation and Measurement, 2020, 69(9): 5981–5983.
[23] WANG X L, ZHANG Y F, ZHANG H X, et al. Radio frequency signal identification using transfer learning based on LSTM. Circuits, Systems, and Signal Processing, 2020, 39(11): 5514–5528.
[24] WU Z L, ZHAO Y L, YIN Z D, et al. Jamming signals classification using convolutional neural network. Proc. of the International Symposium on Signal Processing and Information Technology, 2017: 62−67.
[25] LI X J, FU D, MOU W H, et al. An identification method of navigation signal interference type based on squeezenet model. Proc. of the IEEE 9th Joint International Information Technology and Artificial Intelligence Conference, 2020: 875−880.
[26] SHARMA V, PAREY A. A review of gear fault diagnosis using various condition indicators. Procedia Engineering, 2016, 144: 253–263.
[27] BOASHASH B. Estimating and interpreting the instantaneous frequency of a signal—part 1: fundamentals. Proceedings of the IEEE, 1992, 80(4): 520–538.
[28] BOASHASH B. Estimating and interpreting the instantaneous frequency of a signal—part 2: algorithms and applications. Proceedings of the IEEE, 1992, 80(4): 540–568.
[29] VAKKURI A, YLI-HANKALA A, TALJA P, et al. Time-frequency balanced spectral entropy as a measure of anesthetic drug effect in central nervous system during sevoflurane, propofol, and thiopental anesthesia. Acta Anaesthesiologica Scandinavica, 2004, 48(2): 145–153.
[30] PAN Y N, CHEN J, LI X L. Spectral entropy: a complementary index for rolling element bearing performance degradation assessment. Proceedings of the Institution of Mechanical Engineers, Part C: Journal of Mechanical Engineering Science, 2009, 223(5): 1223–1231.
[31] SAXE A M, MCCLELLAND J L, GANGULI S. Exact solutions to the nonlinear dynamics of learning in deep linear neural networks. Statistics, 2014, 3(1): 1–22.

Biographies

FU Dong was born in 1997. He received his B.S. degree at the College of Intelligence Science and Technology, National University of Defense Technology (NUDT), Changsha, China, in 2019. He is currently pursuing his M.S. degree at the College of Electronic Science and Technology, NUDT. His research interests include GNSS jamming and anti-jamming, satellite navigation time, and frequency technology.
E-mail: fudong@nudt.edu.cn

LI Xiangjun was born in 1997. He received his B.S. degree at the College of Electronic Science and Technology, National University of Defense Technology (NUDT), Changsha, China, in 2019. He is pursuing his M.S. degree at the College of Electronic Science and Technology, NUDT. His research interest is satellite navigation and positioning.
E-mail: 809706022@qq.com

MOU Weihua was born in 1979. He received his Ph.D. degree from National University of Defense Technology (NUDT), Changsha, China, in 2017. He is a professor and master's supervisor at the College of Electronic Science and Technology, NUDT. His main research interests include GNSS signal processing, GNSS signal simulation, and GPU parallel computing.
E-mail: drmou@163.com

MA Ming was born in 1989. He received his Ph.D. degree from College of Electronic Science and Technology, National University of Defense Technology (NUDT), Changsha, China, in 2018. He is a lecturer in NUDT. His research interests include GNSS anti-jamming and time and frequency technology.
E-mail: maming@nudt.edu.cn

OU Gang was born in 1969. He is a professor in the College of Electronic Science and Technology, National University of Defense Technology. He has over 20 years of experience in satellite navigation system research areas including high performance GNSS baseband chip and receiver design and GNSS test and evaluation technology.
E-mail: Ougangcs@139.com